Available online at www.sciencedirect.com
ScienceDirect
Tetrahedron: Asymmetry
Tetrahedron: *Asymmetry* 19 (2008) 568–576

Insight into the mechanism of the Michael addition of malononitrile to α,β-unsaturated imides catalyzed by bifunctional thiourea catalysts

Dongju Zhang,* Guixiu Wang and Rongxiu Zhu

Key Lab of Colloid and Interface Chemistry, Ministry of Education, School of Chemistry and Chemical Engineering, Shandong University, Jinan 250100, PR China

Received 20 December 2007; accepted 29 January 2008

Abstract—The Michael addition of malononitrile to an α,β-unsaturated imide catalyzed by a bifunctional-thiourea catalyst, which represents a prototype of catalytic asymmetric C–C forming reactions, has been investigated by performing density functional theory calculations. Two enantioselective reaction channels, denoted as (*R*)- and (*S*)-channels, which refer to the (*R*)- and (*S*)-configurations of the Michael adducts, have been explored in detail. It was shown that the formation of the Michael adduct involves three elementary steps: the catalyst protonation, the C–C bond coupling, and the catalyst deprotonation. The C–C bond coupling step has been identified as the energetic bottleneck along each channel. The calculated barrier for each of the three elementary steps along the (*R*)-channel is considerably less energy demanding than the corresponding those along the (*S*)-channel. Factors contributing to the high enantioselectivity have been clarified. The present results provided by our calculations are in agreement with all experimental findings and allow a detailed and consistent view of the mechanistic details of this important reaction sequence.

1. Introduction

Inspired by the highly efficient catalysis of multifunctional enzymes, chemists have developed metal-based bifunctional Lewis acid–Lewis base catalysts for asymmetric syntheses.[1,2] However, metal-based catalysts are generally poisonous,[3] and the Lewis acid moiety in these catalysts binds the basic site of substrates too strongly,[4] thus limiting their usability in aqueous or other benign environments. Recently, metal-free catalysts have been developed due to their environmentally and biologically friendly characteristics. These catalysts generally possess H-bond donors and Lewis base functionalities in an asymmetric molecular scaffold.[5–7] In particular, recently developed bifunctional thiourea catalysts have gathered much interest due to their excellent enantioselectivity in asymmetric carbon–carbon forming reactions.[8–14]

Owing to its importance in synthetic chemistry, the enantioselective Michael additions to α,β-unsaturated carbonyl compounds have caused great interest.[15–17] Generally, the use of α,β-unsaturated carbonyl compounds as acceptors (electrophiles) for Michael additions is restricted to enones and nitroalkenes, while 1,3-dicarbonyl compounds are employed as nucleophiles.[18,19] Recently, Jacobsen et al.[20] and Kanemasa et al.[21] have extended the general acceptors to encompass α,β-unsaturated imides and have realized the Michael addition to them using malononitrile (an equivalent to a 1,3-dicarbonyl compound) as a nucleophile with metal-based catalysts. More recently, Takemoto et al.[22] reported this catalytic Michael addition again using alternative bifunctional thiourea organocatalysts. They found that the reaction proceeded with high enantioselectivity [up to 93% ee, with major (*R*)-configuration adduct]. From the ^{1}H NMR spectra experiments, they observed binary complexes between imides and catalysts, which essentially involve a bidentate hydrogen-bond interaction (see Scheme 1). Furthermore, they proposed a plausible transition state structure, where the nucleophilic carbon on the anion of the malononitrile attacks the electron-deficient carbon of the imide to form the desired Michael adduct (refer to panel B of Scheme 3 in Ref. 22). Despite the remarkable achievements on the experimental side for the important Michael addition, our knowledge about the mechanistic details still remains a puzzle, and the role of the active sites of the catalysts in the catalytic process as well as the origin of high enantioselectivity are not yet clearly established. In fact, an explicit and complete elucidation of all elementary steps involved in the reaction is experimentally not

* Corresponding author. E-mail: zhangdj@sdu.edu.cn

0957-4166/$ - see front matter © 2008 Elsevier Ltd. All rights reserved.
doi:10.1016/j.tetasy.2008.01.042

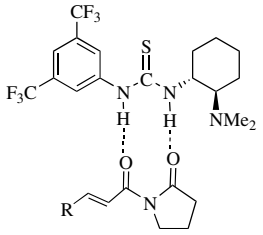

Scheme 1. Schematic diagram of the bidentate hydrogen-bond complex between the thiourea and imide.

possible. This indicates the need for a theoretical assistance to better understand the Michael addition and rationalize the experimental observations. We have thus initiated the present theoretical investigation of the Michael addition of malononitrile to a representative α,β-unsaturated imide catalyzed by a typical bifunctional thiourea catalyst, as shown in Scheme 2. Herein, we unravel the mechanistic details and the origin of high enantioselectivity by performing density functional theory (DFT) calculations, from which we expect to provide a close collaboration between experiment and theory and hence further promote the development of catalytic asymmetric formation of a carbon–carbon bond in organic synthetic chemistry.

2. Models and computational details

As shown in Scheme 1, the system under consideration is rather complex and thus computationally very expensive for carrying out accurate quantum chemistry calculations. In order to reduce computational costs, we have used a truncated form of the bifunctional-thiourea catalyst, where the 3,5-bis(trifluoromethyl) phenyl group was replaced by a hydrogen atom, as shown in Scheme 3. Such simplification is expected to be appropriate enough since the truncated group is not part of the active sites of the Michael addition and plays a less important role during the reaction, while the imide and malononitrile molecules are sufficiently small that we can use their whole forms in the present calculations. For the sake of convenience, the simplified catalyst and imide, as well as malononitrile will be hereafter denoted as **1**, **2**, and **3**, respectively.

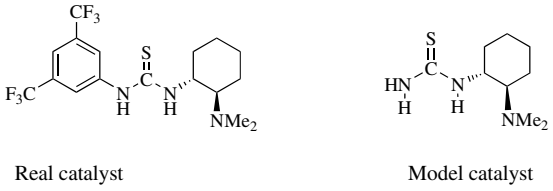

Real catalyst Model catalyst

Scheme 3. Real and simplified catalysts.

Our calculations were carried out within the framework of density functional theory (DFT). The hybrid functional B3LYP[23,24] was chosen in view of its successful performance in modeling organic compound systems, as demonstrated in numerous papers.[25,26] All species involved in the reaction, including reactants, products, minima, and transition states, were first optimized using the standard 6-31G basis set supplemented with polarization functionals only for the key atoms which are directly involved in the reaction processes. The polarization orbital exponents used in our calculations are 1.1, 0.6, 1.154, and 0.864 for H, C, O, and N atoms, respectively. To obtain relatively reliable results, optimization calculations were refined using the more extended basis set 6-31G(d,p) for all atoms. Once the stationary points were obtained at the B3LYP/6-31G(d,p) level, the harmonic vibrational frequencies were calculated at the same level to identify their nature (minima or first-order saddle-points) and to provide zero-point vibrational energy (ZPE) corrections. The intrinsic reaction coordinate (IRC)[27] paths were traced in order to verify the pathways between the transition states and the corresponding minima. The atomic charge assignments were based on natural population analysis (NPA). The GAUSSIAN 03 program package[28] has been used throughout the calculations. Zero-point vibrational energies (ZPE) have been included for all energies cited.

3. Results and discussion

3.1. Catalyst and substrates

The molecular structure of the bifunctional thiourea catalyst shown in Scheme 1 has recently been discussed in detail

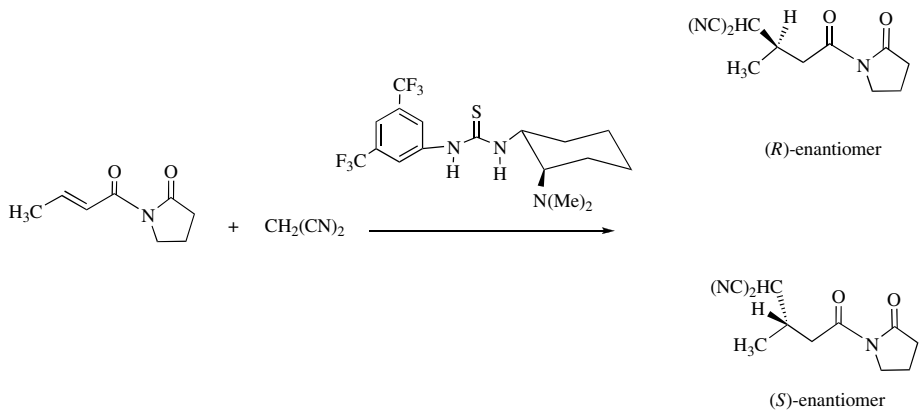

(*R*)-enantiomer

(*S*)-enantiomer

Scheme 2. Asymmetric Michael addition of malononitrile to the α,β-unsaturated imide catalyzed by a bifunctional thiourea catalyst.

by Hamza et al.[29] Several stable structures on the conformational landscape have been located by performing a detailed conformational analysis. They found that the interconversion barriers between the optimal conformers are low (5.4–12.8 kcal mol^{-1}), indicating that the dynamic equilibrium between them can be easily achieved at room temperature. Hence, as generally accepted, they proposed that the catalyst in solution may prefer the particular conformation with the two N–H bonds of the thiourea unit and the amino group pointing in the same direction to efficiently activate the substrates, although it is not the most energetically favorable form in the gas phase. A so-oriented catalyst structure was confirmed to be the most efficient for stabilizing its adducts with substrates. Furthermore, such a conformation is also consistent with the X-ray crystallographic structure of the catalyst.[30] Therefore, the isomer of **1** with two N–H bonds of thiourea unit and the amino group oriented in the same direction was used as the appropriate geometry. Its optimized structure (Fig. 1) shows an intramolecular N–H···N hydrogen bond of 2.191 Å, which is much shorter than that in the solid state (2.70 Å) but in fair agreement with the recently reported theoretical value (2.15 Å) by Hamza et al.[29] It should be noted that the H–N–N–H dihedral angle was calculated to be 46.3°, indicating that the two N–H bonds are out of plane.

For substrate **2**, it is necessary that the two carbonyls are oriented in the same direction in order to be activated via the double H-bond coordination with **1**. As shown in Figure 1, the two carbonyls are almost parallel and the O–C–C–O dihedral is only 13.7°. For the present system, experimental geometrical parameters are only available for substrate **3**. As shown in Figure 1, the theoretical values are in good agreement with the corresponding experimental findings, thus insuring the reliability of our chosen computational level.

3.2. Substrate–catalyst association

The appropriate substrate–catalyst association is crucial for efficiently activating substrates. To establish the optimal arrangement between catalyst **1** and substrates **2** and **3**, we optimized the binary complexes between them, which will be denoted as **1**–**2** and **1**–**3**, respectively. For **1**–**2**, our calculations predicated two stable complexes, **1**–**2**(**I**) and **1**–**2**(**II**), each of which involves a bidentate hydrogen-bond interaction with the dicarbonyl group in **2** as a hydrogen-bond acceptor and the thiourea unit of **1** as a hydrogen-bond donor. In **1**–**2**(**I**), the dicarbonyl group unit is nearly perpendicular to the thiourea unit, in contrast to the almost coplanar arrangement in **1**–**2**(**II**). As shown in Figure 2, the bidentate H-bond distances in **1**–**2**(**I**) are 2.019, 2.261, and 2.283 Å, while they are 2.049, 2.349, and 2.164 Å in **1**–**2**(**II**). It should be noted that an additional, relatively weak C–H···N hydrogen bond with a H···N distance of 2.474 Å exists in **1**–**2**(**I**), which may be the reason that

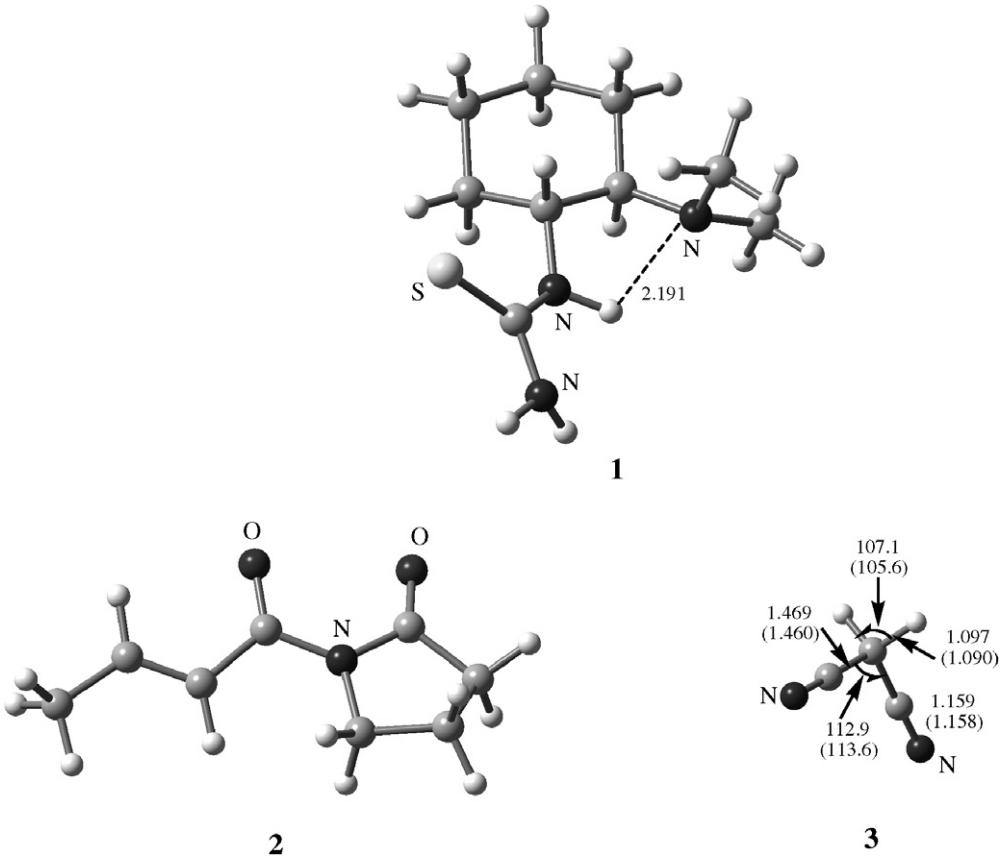

Figure 1. Optimized geometries for catalyst **1**, imide **2** and malononitrile **3** with selected bond lengths (in Å) and angles (°).

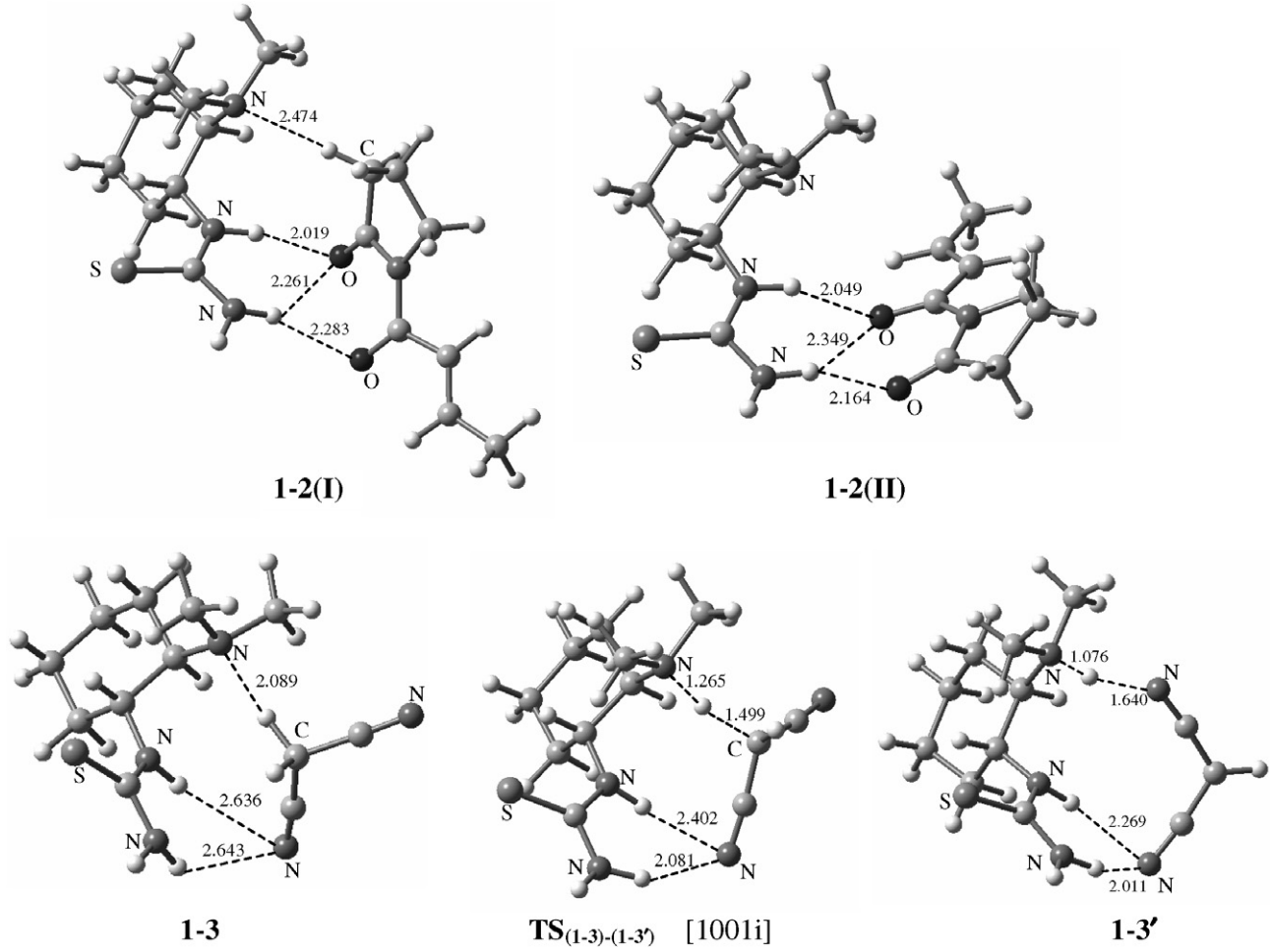

Figure 2. Optimized geometries for the binary complexes of the catalyst **1** with imide **2** and malononitrile **3** with selected bond lengths (in Å). The value in the square brackets denotes the imaginary frequency.

1–**2**(**I**) is slightly more favorable in energy than **1**–**2**(**II**). The formation of these H bonds supplies stabilization energies of 10.50 and 9.89 kcal mol^{-1} for **1**–**2**(**I**) and **1**–**2**(**II**). For **1**–**3**, the most stable structure is characterized by the main N···H–C hydrogen bond of 2.089 Å and a relatively weaker bifurcated N–H···N hydrogen bond, as shown in Figure 2. The binding energy of this complex is calculated to be 6.84 kcal mol^{-1}, which is 3.66 kcal mol^{-1} smaller than that of **1**–**2**(**I**). This fact indicates that the catalyst prefers to associate with **2** rather than **3**, which may be the reason why the binary complex of the catalyst with the imide could be spectroscopically detected, while the corresponding complex with malononitrile was not observed in the ^{1}H NMR spectrum experiment.[22]

3.3. Generation of malononitrile anion

According to the mechanism proposed by Takemoto,[22] the formation of malononitrile anion provides the active nucleophilic carbon, promoting the ensuring C–C bond coupling. The formation of this anion is, in fact, a deprotonation process of **3** by the basic amine group in **1**. It is known that both hydrogens on the methylene in **3** are active due to the strong electro-withdrawing character of CN group, and thus it is easily deprotoned via a proton transfer from the methylene to the amine group of **1**, as confirmed by the calculated small energy barrier (10.55 kcal mol^{-1}) of this process. The optimized transition state structure related to this process is shown in Figure 2, denoted as $\mathbf{TS}_{(\mathbf{1}\text{–}\mathbf{3})\text{–}(\mathbf{1}\text{–}\mathbf{3}')}$, where the thiourea unit of **1** stabilizes the structure via bifurcated hydrogen bonds. Following the forward IRC calculations from $\mathbf{TS}_{(\mathbf{1}\text{–}\mathbf{3})\text{–}(\mathbf{1}\text{–}\mathbf{3}')}$, we have located an ion pair structure **1**–**3**′, where the deprotonated **3** is reoriented so as to form a more stable N–H···N hydrogen-bond-containing complex, as shown in Figure 2. At the present theoretical level, **1**–**3**′ is found to be 5.99 kcal mol^{-1} more stable than **1**–**3**.

3.4. Ternary complexes

The above analysis has actually provided an initial guidance for understanding the Michael addition. It appears that the thiourea unit of **1** activates **2** via multiple H bonds to enhance the electrophilic character of the carbon center as an acceptor, while its amine group interacts with **3** to generate the nucleophilic carbon center as the donor. To confirm this conjecture, we studied the geometry of the ternary complex among **1**, **2**, and **3**. Two isomers are obtained

by attaching **3** to **1**–**2**(**I**) and **1**–**2**(**II**) with a H on the methylene approaching the N atom on the amine group. Such ternary complexes will be denoted as **IM1**(***R***) and **IM1**(***S***), which means that the initial (*R*)- and (*S*)-configuration intermediates form (*R*)- and (*S*)-configuration adducts. The optimized geometries of **IM1**(***R***) and **IM1**(***S***) are shown in Figures 3 and 4, respectively, both of which are characterized by multiple H bonds, including the bifurcated H bonds between the diketone group in **2** and the thiourea unit of **1**, and the normal H bond between the amine group of **1** and the H atom in the methylene of **3**. **IM1**(***R***) and **IM1**(***S***) were found to be more stable by 21.23 and 20.36 kcal mol^{-1} in energy, relative to their separated species, respectively. These ternary complexes are considered as appropriate precursors to the C–C bond coupling reaction.

3.5. C–C bond formation

In this section, we explore the C–C bond formation mechanism along the two enantioslective channels, (*R*)- and (*S*)-channels, which correspond to the formation of the (*R*)- and (*S*)-configuration Michael adducts, respectively. Figures 3 and 4 show the optimized geometries of minima and transition states along these two channels, and the corresponding potential energy surfaces profiles are given in Figure 5. We found that the mechanisms along the two channels are very similar to each other, so it is only necessary to describe one of them in detail, that is, the (*R*)-channel. As shown in Figure 5, the C–C bond formation involves three elementary steps: the catalyst protonation, the C–C bond coupling, and the catalyst deprotonation.

The catalyst protonation involves the proton migration from the methylene to the amine group. In this process, **IM1**(***R***) is converted to **IM2**(***R***) via transition state $\mathbf{TS_{1-2}}$(***R***), where the C–H bond (1.445 Å) on the methylene is breaking, while the N–H bond (1.314 Å) is forming. The calculated barrier for this process is only 6.94 kcal mol^{-1}, similar to that (10.55 kcal mol^{-1}) found in the deprotonation process of **3** by **1** without the presence of **2**. This indicates that even in the ternary complex, the proton migration can take place easily, that is, the presence of **2** does not cause steric hindrance to the deprotonation process. It should be noted that **IM2**(***R***) is stabilized via a N–H···N hydrogen bond with an H···N distance of

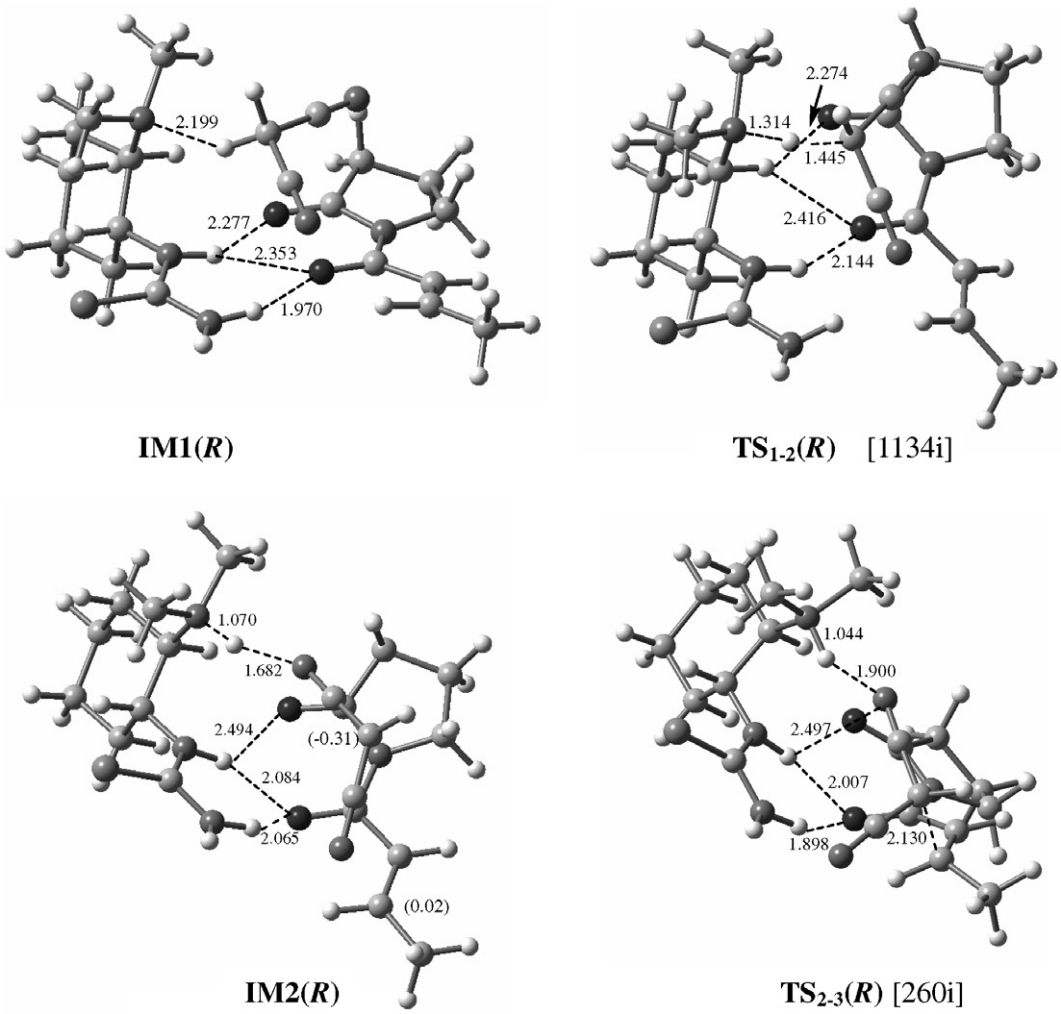

Figure 3. Optimized structures with selected bond distances (in Å) for the stationary points located along the (*R*)-enantioselective channel. The values in parentheses in **IM2**(***R***) denote the NPA charge on the carbon centers to be coupled, and the values in the square brackets denote the imaginary frequency.

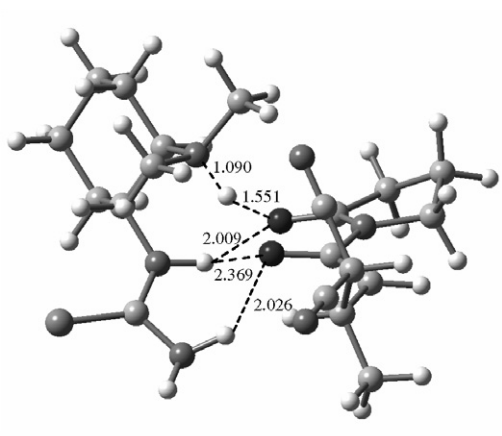

IM3(*R*)

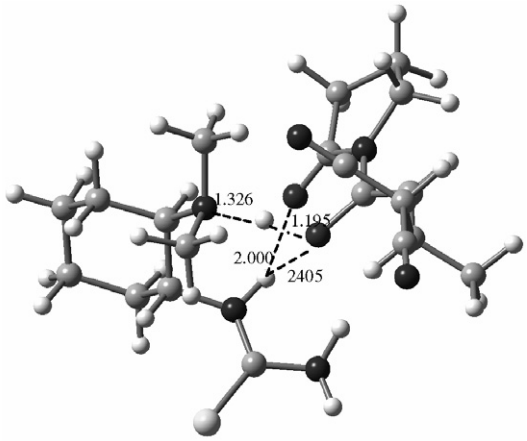

$TS_{3\text{-}4}$(*R*) [761i]

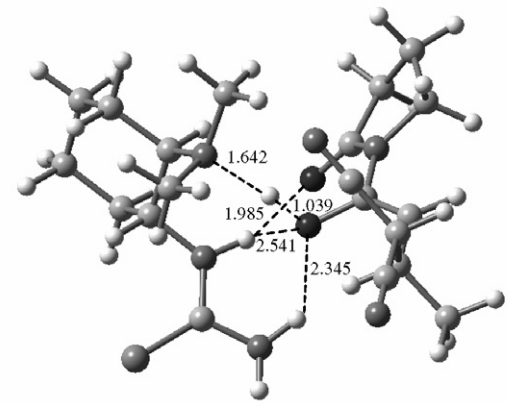

IM4(*R*)

Figure 3. (*continued*)

1.682 Å, indicating that the anionic **3** unit has been reoriented after deprotonation, that is, **1** is able to recognize the substrate to be an optimal position to promote the reaction. The NPA on **IM2**(***R***) shows that the NPA charges on the electrophilic and nucleophilic carbon centers are 0.02 and −0.31 e, in contrast to those in free **2** and **3**, −0.03 and −0.28 e, showing an enhancement in the electrophilicity of **2** and the nucleophilicity of **3** via their binding to **1**.

The following C–C bond coupling between the two carbon centers occurs via transition state $\mathbf{TS_{2\text{–}3}}$(***R***), where the distance of the forming C–C is 2.130 Å and the transition vector corresponds to the expected components of the reaction coordinate. Our calculations show a moderate energy barrier (11.43 kcal mol^{-1}) for this coupling process. By comparing the H-bond distances in $\mathbf{TS_{2\text{–}3}}$(***R***) with those in **IM2**(***R***), we find that the bidentate H-bond is strengthened while the N–H··N hydrogen bond is weakened. This can be attributed to the charge transfer from the nucleophilic center to the electrophilic center and the following charge delocalization. In fact, the NPA can quantify this change with charge values for the two carbonyl oxygens and for the cyano-nitrogen adjacent to the proton. They are −0.633, −0.605, and −0.633 e in **IM2**(***R***) and −0.706, −0.660, and −0.501 e in $\mathbf{TS_{2\text{–}3}}$(***R***), respectively. From the forward IRC calculation from $\mathbf{TS_{2\text{–}3}}$(***R***) we obtained **IM3**(***R***), which is efficiently stabilized by the multiple H bonds and lies 16.24 kcal mol^{-1} below the entrance. **IM3**(***R***) is actually a binary complex between protonated **1** and the Michael adduct.

Finally, the Michael adduct can be obtained via the catalyst deprotonation by **1**. It is noteworthy that in **IM3**(***R***) there is a strong H bond between the protoned amine group and the carbonyl oxygen, as indicated by the short N–H···O H bond distance of 1.551 Å. As a result, the proton may prefer to transfer to the carbonyl oxygen rather than to the methylene carbon to form the enol isomer of the Michael addition. Our calculations show that the proton migration to the carbonyl oxygen can take place very easily, and the barrier related to this process was found to be only 0.19 kcal mol^{-1}. As shown in Figure 3, we have located the transition state structure related to the deprotonation process, $\mathbf{TS_{3\text{–}4}}$(***R***), and the IRC calculation shows that it connects **IM3**(***R***) and **IM4**(***R***). **IM4**(***R***), a product-like precursor, lies 16.60 kcal mol^{-1} below the entrance,

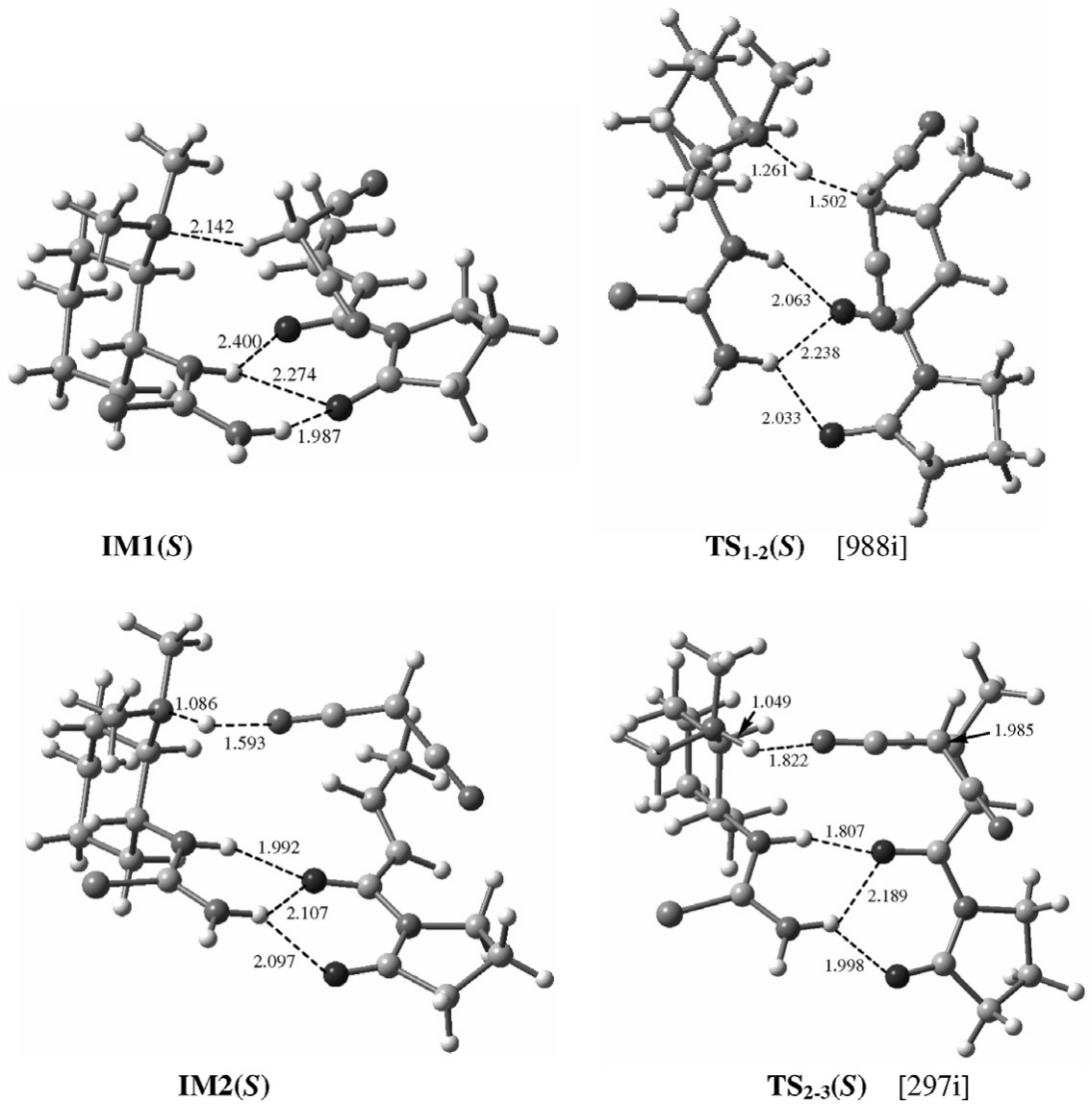

Figure 4. Optimized structures with selected bond lengths for the stationary points located along the (*S*)-enantioselective channel. The values in the square brackets denote the imaginary frequency.

and its direct dissociation can result in the formation of an (*R*)-configuration of the enol Michael adduct (denoted as **P** in Fig. 5) and the release of catalyst **1**.

It should be noted that all stationary points involved in the above three elementary steps involve multiple H bonds, which organize the catalyst and substrates to their optimal arrangements so that both the substrates are activated simultaneously. From the profile of the potential energy surface shown in Figure 5, it is clear that the C–C bond coupling step is the rate-determining step to form the Michael adduct. The mechanism details along the (*S*)-channel are nearly the same as those along the (*R*)-channel, meaning that we only show the related results in Figures 4 and 5 without detailed description. However, one thing that should be noted is that along the (*S*)-channel, the energy demanded in going from **IM3**(***S***) to $\mathbf{TS_{3-4}}(\boldsymbol{S})$ is only 0.46 kcal mol^{-1}, and in fact, adding ZPE correction reverses their order, so that $\mathbf{TS_{3-4}}(\boldsymbol{S})$ is actually lower in energy by 2.77 kcal mol^{-1}. This suggests that the potential energy surface around this area is very flat and the corresponding catalyst deprotonation can occur easily.

3.6. Enantioselectivity

From Figure 5, it is apparent that all the stationary points along the *R*-channel lie lower than those along the (*S*)-channel. The barriers of the three elementary steps involved in the Michael addition are 6.94, 11.43, and 0.19 kcal mol^{-1} along the (*R*)-channel, while those along the (*S*)-channel are 10.43, 16.62, and −2.77 kcal mol^{-1}. In particular, the barrier of the rate-determining step (C–C bond coupling process) for the former is 5.19 kcal mol^{-1} more favorable than the latter. This fact indicates that the Michael addition occurs predominantly along the (*R*)-channel, which supports the experimentally observed high enantioselectivity with the major (*R*)-configuration of the Michael adduct. To better understand this enantioselectivity, we focused our attention on the geometrical characteristics of the stationary points involved along the two

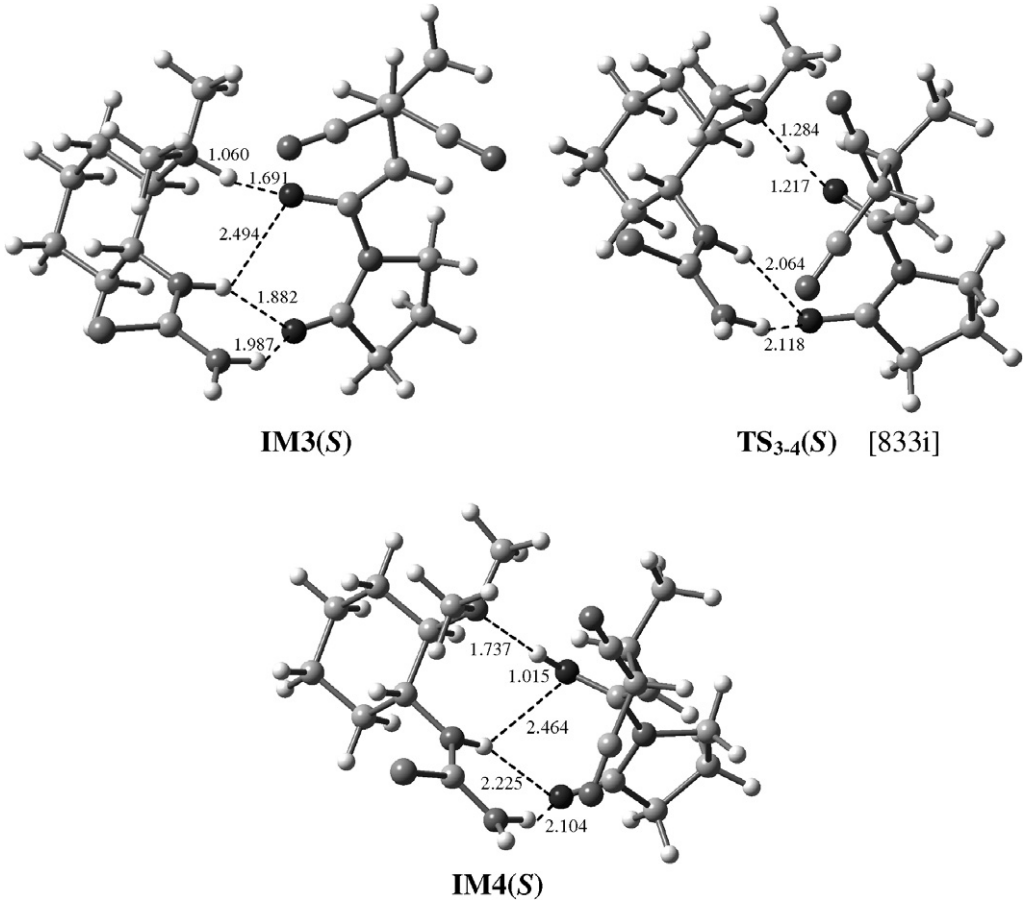

Figure 4. (*continued*)

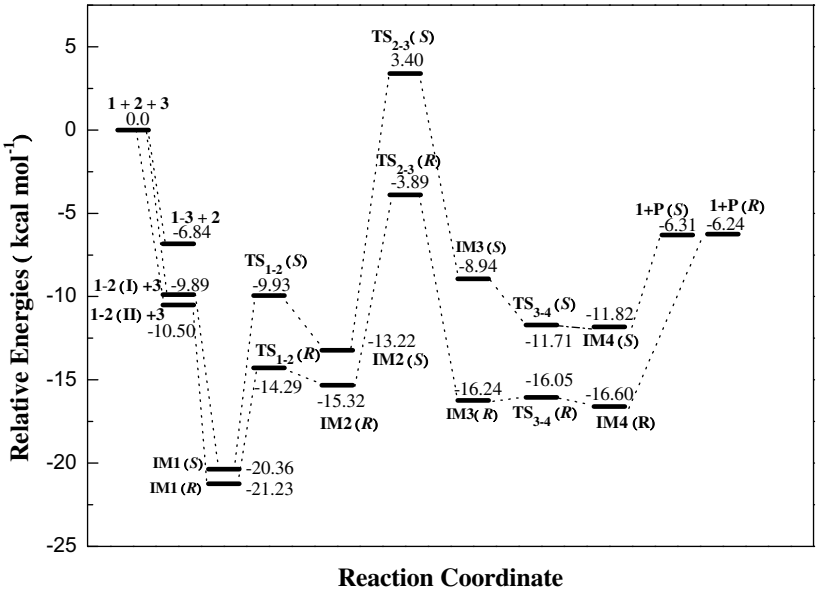

Figure 5. Profiles of the potential energy surfaces for the Michael addition of malononitrile **3** to imide **2** catalyzed by the bifunctional thiourea **1** along both the (*R*)- and (*S*)-enantioselective channels. Zero point vibrational energies (ZPE) have been included for all energies cited.

channels. Taking $\mathbf{TS_{2-3}}(\boldsymbol{R})/\mathbf{TS_{2-3}}(\boldsymbol{S})$ (the transition state structure of the rate-determining step along each channel) for example, we studied their geometrical arrangements in detail and found out a few effects that contribute to

the enantioselectivity of the reaction. First, it was noticed that the static repulsion between units **2** and **3** around the area of the forming C–C bond plays an important role. The staggered conformation of the C–C≡N group and the C=C bond in $\mathbf{TS_{2-3}}(\boldsymbol{R})$ results in its higher stability relative to $\mathbf{TS_{2-3}}(\boldsymbol{S})$, in which the two groups are in an eclipsed conformation instead. Another factor that controls the enantioselectivity is the electronic repulsion between the two carbon centers, which is developing into the C–C bond of the Michael adduct. Accordingly, the C–C distance in $\mathbf{TS_{2-3}}(\boldsymbol{R})$ (2.130 Å) is relatively larger than that in $\mathbf{TS_{2-3}}(\boldsymbol{S})$ (1.985 Å), thus making $\mathbf{TS_{2-3}}(\boldsymbol{R})$ energetically more favorable than $\mathbf{TS_{2-3}}(\boldsymbol{S})$. Lastly, the N–H···N hydrogen bond has an important effect on the enantioselectivity, which results in the delocalization of the negative charge on the nucleophile and thus is unfavorable for the C–C bond coupling. As demonstrated by the calculated geometrical parameters, such an H-bond interaction in $\mathbf{TS_{2-3}}(\boldsymbol{R})$ is weaker than that in $\mathbf{TS_{2-3}}(\boldsymbol{S})$, leading to a lower energy of $\mathbf{TS_{2-3}}(\boldsymbol{R})$ relative to $\mathbf{TS_{2-3}}(\boldsymbol{S})$. The interplay between these effects ultimately determines the high enantioselectivity of the Michael addition with the main (*R*)-enantiomer.

4. Conclusions

In conclusion, our DFT calculations provide the key basis for understanding the Michael addition of malononitrile to α, β-unsaturated imides catalyzed by bifunctional thiourea catalysts. It is shown that docking both the acceptor and the donor of the Michael addition into the active sites of the catalyst is achieved via intermolecular hydrogen-bonds. The two enantioselective reaction channels leading to the (*R*)- and (*S*)-Michael adducts have been determined in detail. Along both the (*R*)- and (*S*)-channels, the Michael addition proceeds via three elementary steps (the protonation of the catalyst, C–C bond coupling, and deprotonation of the catalyst), while the (*R*)-channel is found to be energetically more favorable than the (*S*)-channel through each elementary step. The factors contributing to the high enantioselectivity have been clarified. The present results rationalize the experimental findings well, and also would stimulate further research toward the asymmetric Michael addition for an ever-widening range of synthesis both experimentally and theoretically.

Acknowledgment

The work described in this paper was fully supported by the National Natural Science Foundations of China (Grant No. 20773078).

References

1. Strater, N.; Lipscomb, W. N.; Klabunde, T.; Krebs, B. *Angew. Chem., Int. Ed.* **1996**, *35*, 2024–2055.
2. Sammis, G. M.; Danjo, H.; Jacobsen, E. N. *J. Am. Chem. Soc.* **2004**, *126*, 9928–9929.
3. Berkessel, H.; Gröger, H. *Asymmetric Organocatalysis*; Wiley-VCH: Weinheim, Germany, 2005.
4. Schreiner, P. R. *Chem. Soc. Rev.* **2003**, *32*, 289–296.
5. Houk, K. N., List, B., Eds. *Acc. Chem. Res.* **2004**, *37*, 487–631.
6. Dalko, P. I.; Moisan, L. *Angew. Chem., Int. Ed.* **2004**, *43*, 5138–5175.
7. Taylor, M. S.; Jacobsen, E. N. *Angew. Chem., Int. Ed.* **2006**, *45*, 1520–1543.
8. Okino, T.; Hoashi, Y.; Takemoto, Y. *J. Am. Chem. Soc.* **2003**, *125*, 12672–12673.
9. Hoashi, Y.; Yabuta, T.; Takemoto, Y. *Tetrahedron Lett.* **2004**, *45*, 9185–9188.
10. Connon, S. J. *Chem. Eur. J.* **2006**, *12*, 5418–5427.
11. Li, H.; Zu, L.; Wang, J.; Wang, W. *Tetrahedron Lett.* **2006**, *47*, 3145–3148.
12. Mattson, A. E.; Zuhl, A. M.; Reynolds, T. E.; Scheidt, K. A. *J. Am. Chem. Soc.* **2006**, *128*, 4932–4933.
13. Tsogoeva, S. B.; Wei, S. B. *Chem. Commun.* **2006**, 1451–1453.
14. Yalalov, A.; Tsogoeva, S. B.; Schmatz, S. *Adv. Synth. Catal.* **2006**, *348*, 826–832.
15. Sibi, M. P.; Manyem, S. *Tetrahedron* **2000**, *56*, 8033–8061.
16. Fagnou, K.; Lautens, M. *Chem. Rev.* **2003**, *103*, 169–196.
17. Taylor, M. S.; Zalatan, D. N.; Lerchner, A. M.; Jacobsen, E. N. *J. Am. Chem. Soc.* **2005**, *127*, 1313–1317.
18. Sundararajan, G.; Prabagaran, N. *Org. Lett.* **2001**, *3*, 389–392.
19. Watanabe, M.; Ikagawa, A.; Wang, H.; Murata, K.; Ikariya, T. *J. Am. Chem. Soc.* **2004**, *126*, 11148–11149.
20. Taylor, M. S.; Jacobsen, E. N. *J. Am. Chem. Soc.* **2003**, *125*, 11204–11205.
21. Kanemasa, S.; Ito, K. *Eur. J. Org. Chem.* **2004**, *23*, 4741–4753.
22. Hoashi, Y.; Okino, T.; Takemoto, Y. *Angew. Chem., Int. Ed.* **2005**, *44*, 4032–4035.
23. Becke, A. D. *J. Chem. Phys.* **1993**, *98*, 5648–5652.
24. Lee, C.; Yang, W.; Parr, R. G. *Phys. Rev. B* **1988**, *37*, 785–789.
25. Leach, A. G.; Houk, K. N. *J. Am. Chem. Soc.* **2002**, *124*, 14820.
26. Pfaendtner, J.; Yu, X.; Broadbelt, L. J. *J. Phys. Chem. A* **2006**, *110*, 10863.
27. Gonzalez, C.; Schlegel, H. B. *J. Chem. Phys.* **1989**, *90*, 2154–2161.
28. Frisch, M. J.; Trucks, G. W.; Schlegel, H. B.; Scuseria, G. E.; Robb, M. A.; Cheeseman, J. R.; Zakrzewski, V. G.; Montgomery, J. A., Jr.; Stratmann, R. E.; Burant, J. C.; Dapprich, S.; Millam, J. M.; Daniels, A. D.; Kudin, K. N.; Strain, M. C.; Farkas, O.; Tomasi, J.; Barone, V.; Cossi, M.; Cammi, R.; Mennucci, B.; Pomelli, C.; Adamo, C.; Clifford, S.; Ochterski, J.; Petersson, G. A.; Ayala, P. Y.; Cui, Q.; Morokuma, K.; Malick, D. K.; Rabuck, A. D.; Raghavachari, K.; Foresman, J. B.; Cioslowski, J.; Ortiz, J. V.; Baboul, A. G.; Stefanov, B. B.; Liu, G.; Liashenko, A.; Piskorz, P.; Komaromi, I.; Gomperts, R.; Martin, R. L.; Fox, D. J.; Keith, T.; Al-Laham, M. A.; Peng, C. Y.; Nanayakkara, A.; Gonzalez, C.; Challacombe, M.; Gill, P. M. W.; Johnson, B.; Chen, W.; Wong, M. W.; Andres, J. L.; Gonzalez, C.; Head-Gordon, M.; Replogle, E. S.; Pople, J. A. GAUSSIAN 03, *Revision B.05*, Gaussian: Pittsburgh, PA, 2003.
29. Hamza, A.; Schubert, G.; Soos, T.; Papai, I. *J. Am. Chem. Soc.* **2006**, *128*, 13151–13160.
30. Okino, T.; Hoashi, Y.; Furukawa, T.; Xu, X.; Takemoto, Y. *J. Am. Chem. Soc.* **2005**, *127*, 119–125.